Influence of MACl additive on grain boundary, trap-state properties, and charge dynamics in perovskite solar cells

Yanru Guo,[a] Shuai Yuan,[a] Dongping Zhu,[a] Man Yu,[b] Hao-Yi Wang,[a] Jun Lin,[a] Yi Wang,[a] Yujun Qin,[a] Jian-Ping Zhang[a] and Xi-Cheng Ai*[a]*

[a]Department of Chemistry, Renmin University of China, Beijing 100872, China.

[b]School of Materials Engineering, Xi'an Aeronautical University, Xi'an 710077, China.

E-mail: jlin@ ruc.edu.cn (Jun Lin), xcai@ruc.edu.cn (Xi-Cheng Ai)

S1. Perovskite Film Characterization

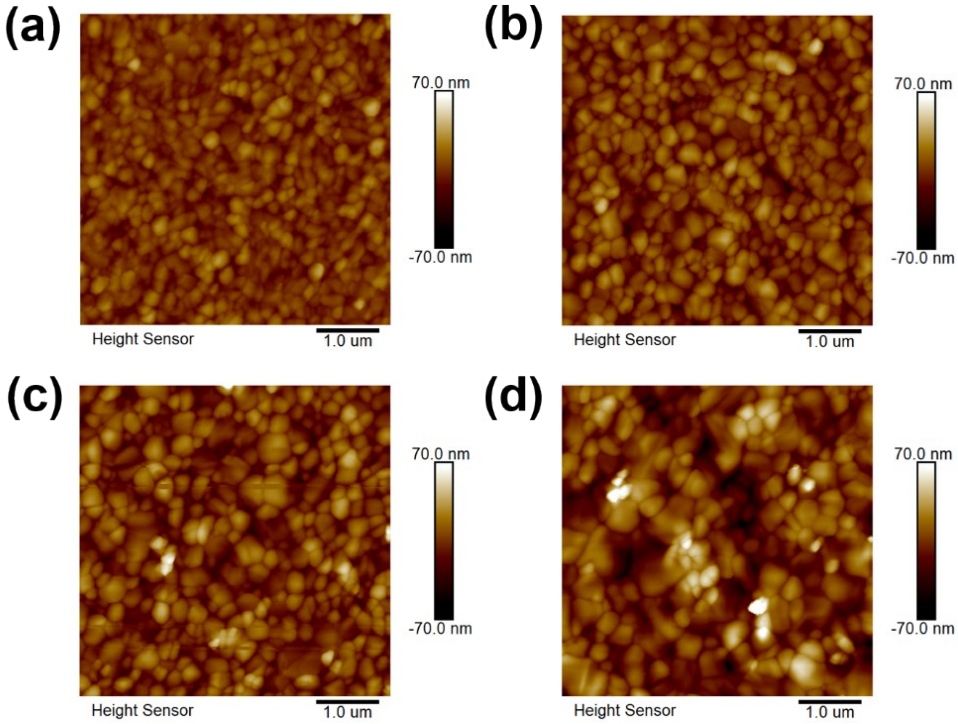

Fig. S1. AFM topographic images of perovskite films: (a) GS-270, (b) GS-410, (c) GS-580 and (d) GS-600.

Table S1. Standard deviation of the grain size distribution for the GS-270, GS-410, GS-580 and GS-600 perovskite films.

Sample	GS-270	GS-410	GS-580	GS-600
Standard deviation	93.66	136.74	179.13	370.72

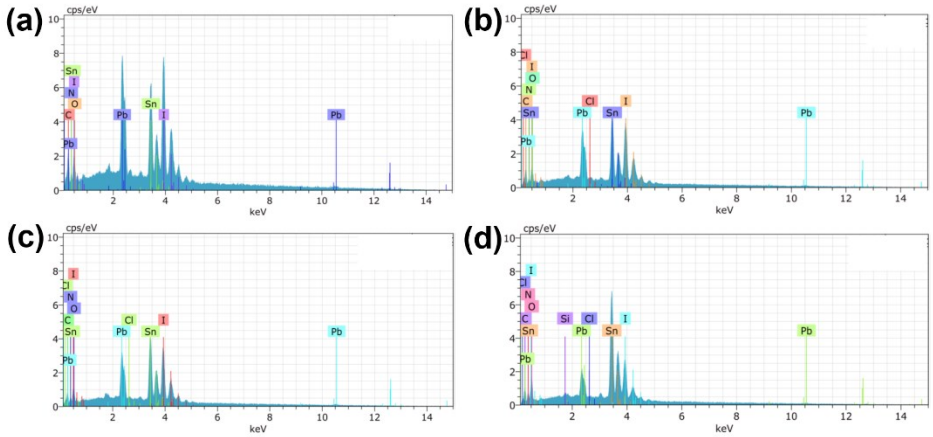

Fig. S2. EDS of perovskite films: (a) GS-270, (b) GS-410, (c) GS-580 and (d) GS-600.

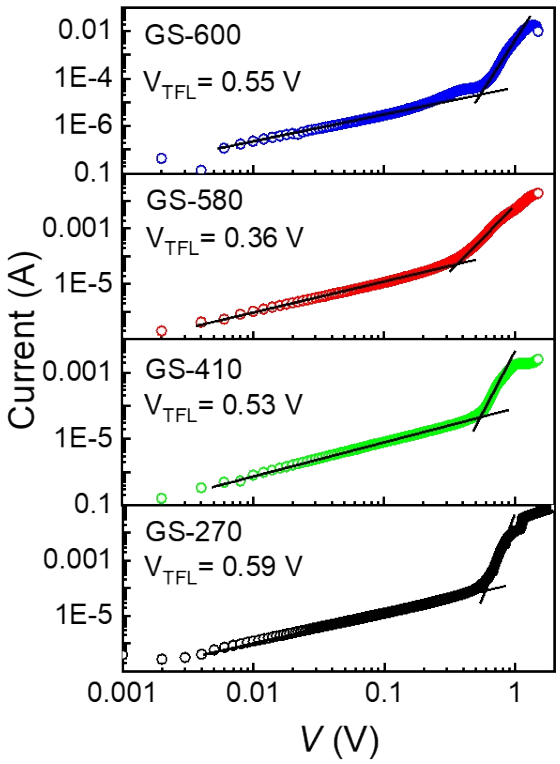

Fig. S3. Current-voltage curves in dark of devices based on perovskite films with different grain size.

The trap density (n_t) can be determined according to the equation:[1,2]

$$n_t = \frac{2V_{TFL}\varepsilon\varepsilon_0}{eL^2} \qquad \text{S1}$$

where ε_0 is the vacuum permittivity, ε is the dielectric constant of $MAPbI_3$, e is the elementary charge and L is the thickness of the perovskite layer.

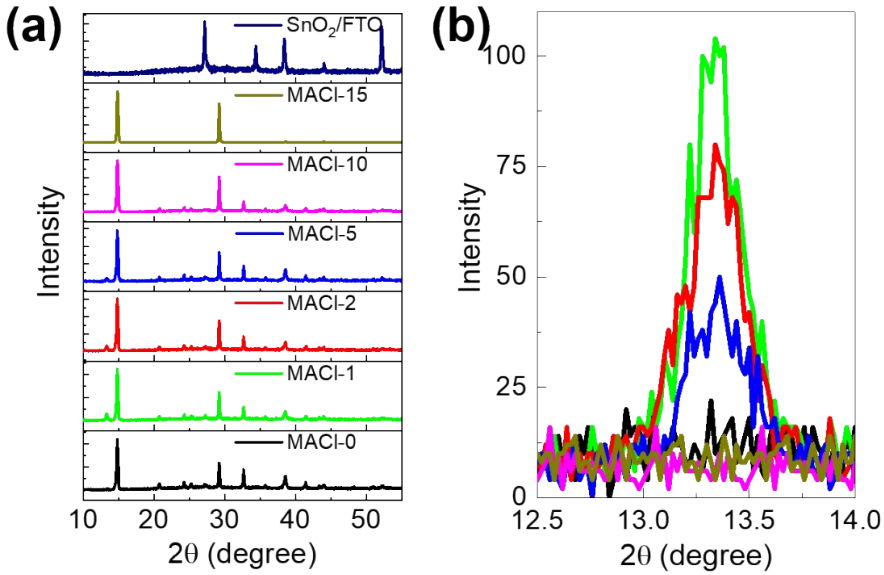

Fig. S4. (a) XRD patterns and (b) zoomed-in PbI_2 diffraction region of perovskite films obtained by adding different MACl contents (0, 1, 2, 5, 10 and 15 mg mL^{-1}).

To further explore the relationship of the PbI_2 residue and PL quenching, various concentrations of MACl additives (x = 0, 1, 2, 5, 10 and 15 mg mL^{-1}) are used to prepare the perovskite films (named MACl-x). According to Fig. S4, all the perovskite films show similar diffraction characteristic peaks of tetragonal perovskite phase. In addition, the perovskite films obtained by introducing a small amount of MACl have the characteristic diffraction peak of PbI_2 at 13.29°, and the PbI_2 peak gradually disappears with the increase of MACl content. It is consistent with XPS result that the binding energy position of Pb 4f moves to higher binding energy with the increase of PbI_2 content in the film (Fig. 3). This is a common phenomenon in perovskite films modified by MACl additive.[3-5] In the perovskites film with inadequate MACl additive (1 mg mL^{-1}), the evaporation of MA leaves cation vacancies and PbI_2 residue.[5] With more MACl additive (2 mg mL^{-1}), the PbI_2 residual amount decreases. The PbI_2 residual gradually disappears with the increase of MACl additive (5, 10, 15 mg mL^{-1}).

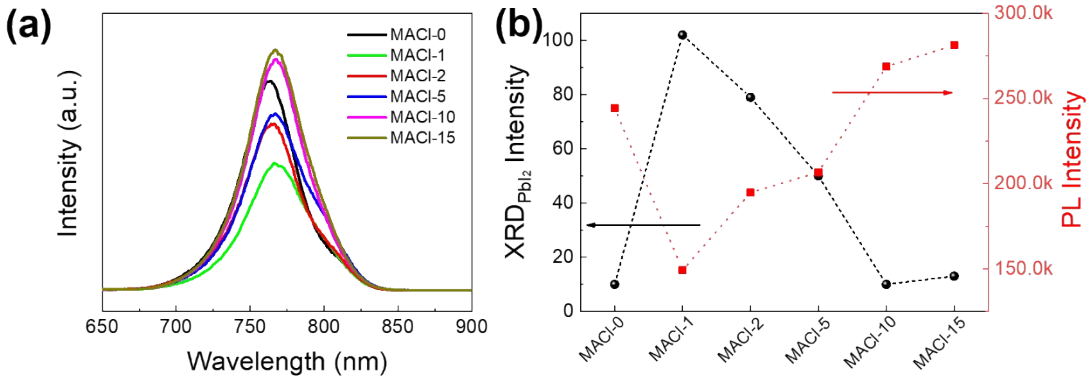

Fig. S5. (a) Steady-state PL spectra and (b) variation trend of PL intensity (right axis) and [001] crystal plane intensity of PbI_2 in XRD patterns (left axis) of perovskite film obtained by adding different MACl content.

The PL spectra of perovskite films obtained by adding different MACl contents (0, 1, 2, 5, 10 and 15 mg mL^{-1}) are shown in Fig. S5a. Overall, the PL intensity decreases initially and then increases with the increase of MACl content from 1 mg mL^{-1} to 15 mg mL^{-1}. Obviously, there is a negative correlation between PL intensity and PbI_2 content as shown in Fig. S5b, indicating that the PbI_2 inhibits the radiative recombination luminescence of the charge in the perovskite. This is because the energy levels of PbI_2 and perovskite are well matched, and there is a heterogeneous charge transfer mechanism from perovskite to PbI_2.[6,7] That is, the electrons on the conduction band of perovskite are partially transferred to the conduction band of PbI_2, which accelerates the charge separation and inhibits the charge radiation recombination in the perovskite.

Table S2. Fitting parameters extracted from the PL decay traces.

Sample	A_1	τ_1 (ns)	A_2	τ_2 (ns)	τ_{ave}
GS-270	0.63	10.78	0.37	26.27	16.51
GS-410	0.34	3.08	0.66	31.32	21.72
GS-580	0.39	3.16	0.61	36.36	23.41

S2. Temperature-Dependent Photoluminescence Spectra

Table S3. The area analysis of fitting peaks extracted from the PL at 78K.

Sample	Peak area (tetragonal)	Peak area (trap of tetragonal)	Area ratio[a]
GS-270	2.50	39.80	15.92
GS-410	2.40	24.30	14.17
GS-580	4.13	30.30	7.36

a: the area ratio of trap of tetragonal to tetragonal.

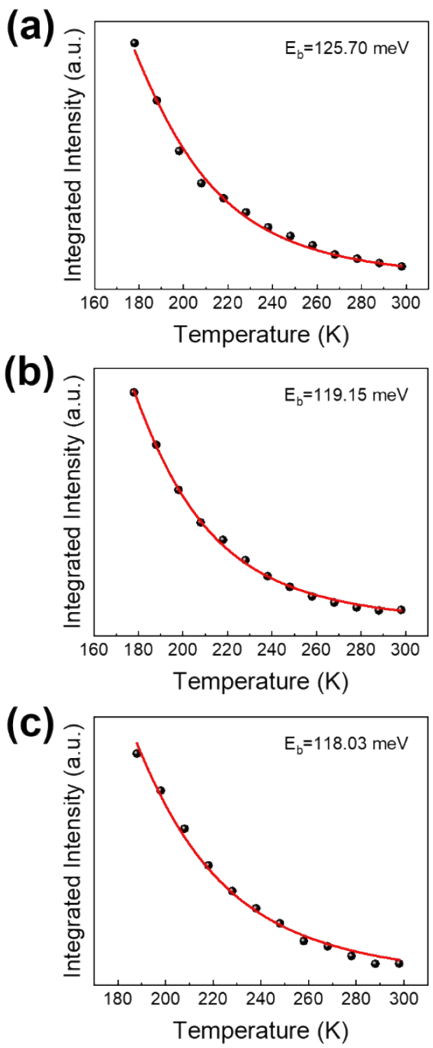

Fig. S6. Temperature-dependent integrated intensities of perovskite films: (a) GS-270, (b) GS-410 and (c) GS-580. The solid red lines are the corresponding fittings.

TDPL spectra has been employed to study the structural and optoelectronic properties of perovskites. Closer inspection of fluorescence spectrum reveals that the emission intensity decreases with increasing the temperature from 168–298 K, as shown in Fig. S6, which can be fitted with the Arrhenius equation,[8]

$$I(T) = \frac{I_0}{1 + Ae^{-\frac{E_b}{k_B T}}} \qquad \text{S2}$$

where I_0 is defined as the integrated emission intensity at T = 0 K, A is the pre-exponential factor, k_B is the Boltzmann constant and E_b is the exciton bonding energy. Based on the fitting results, the approximate E_b values of the three films are determined to be 125.70 meV, 119.15 meV and 118.03 meV for the GS-270, GS-410 and GS-580 perovskite films, respectively. The smaller E_b value of the GS-580 perovskite film is conducive to efficient initial charge separation. This means that it is easy to form free exciton carriers instead of bound exciton carriers.[9] On the contrary, the larger E_b value of the control perovskite film would reduce the charge separation efficiency and is not beneficial to the photovoltaic performance of the PSCs.

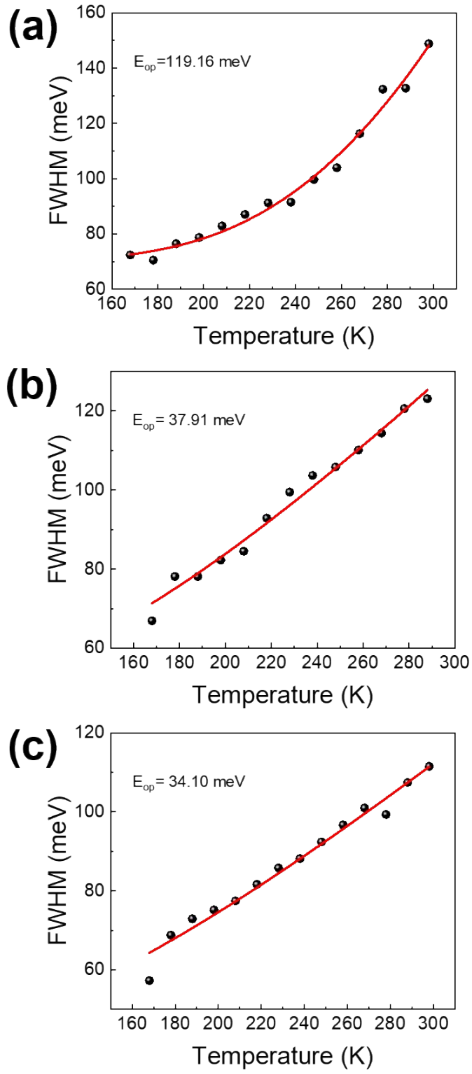

Fig. S7. Temperature-dependent full-width at half-maximum (FWHM) broadening of perovskite film (a) GS-270, (b) GS-410 and (c) GS-580.

The temperature-dependence of the PL peak broadening can provides detailed information on the exciton-phonon coupling in the perovskite, which also strongly influences the excitonic fluorescence emissions.[10] The parameter of FWHM can be converted from nm to meV according to the equation FWHM (meV) = $1.24 \times 10^6 \times$ FWHM(nm)/$\lambda_1\lambda_2$, where λ_1 and λ_2 represent the corresponding fitted starting and end wavelengths of the FWHM. Fig. S7 displays the temperature-dependent emission peak broadening relationship, which can be fitted using the Boson model (equation S3),[11]

$$\Gamma(T) = \Gamma_0 + \sigma T + \frac{\Gamma_{op}}{e^{(E_{op}/k_B T)} - 1} \qquad \text{S3}$$

where Γ_0 is the inhomogeneous broadening contribution, σ and Γ_{op} describe the interactions of exciton-acoustic phonon and exciton-optical phonon contributions to the line width broadening, respectively. E_{op} is the optical phonon energy. Since the contribution from the acoustic phonons is negligible in relation to the optical energy, the parameter of σ can be set to zero for simplicity. The corresponding E_{op} values are calculated to be 119.16 meV, 37.91 meV and 34.10 meV for the GS-270, GS-410 and GS-580 perovskite film, respectively. The smaller E_{op} are favorable for charge transfer in PSCs.

The polaron binding energy (E_p) is calculated based on Fröhlich's weak coupling theory[12],

$$E_p = \alpha E_{op},\ \alpha = \frac{1}{2}\left(\frac{1}{\varepsilon_\infty} - \frac{1}{\varepsilon_0}\right)\left(\frac{1}{\varepsilon_v}\right)\frac{e^2}{h}\sqrt{\frac{m^*}{2E_{op}}}$$

Where ε_∞ = 6.05, ε_0= 25.66 (both are average values), ε_v is permittivity in vacuum, e is the elementary charge, h is the Planck constant, m^* is effective electron mass (0.18 m_e, m_e is the electron mass). The E_p of GS-270, GS-410 and GS-580 are 102.65 meV, 32.66 meV and 29.38 meV, respectively. The results suggest that the perovskite with enlarged grain size and reduced trap-states prefers a relatively larger polaron with larger phonon cloud radius and stronger scatter screening effects compared with the controlled perovskite.

S3. Device Characterization

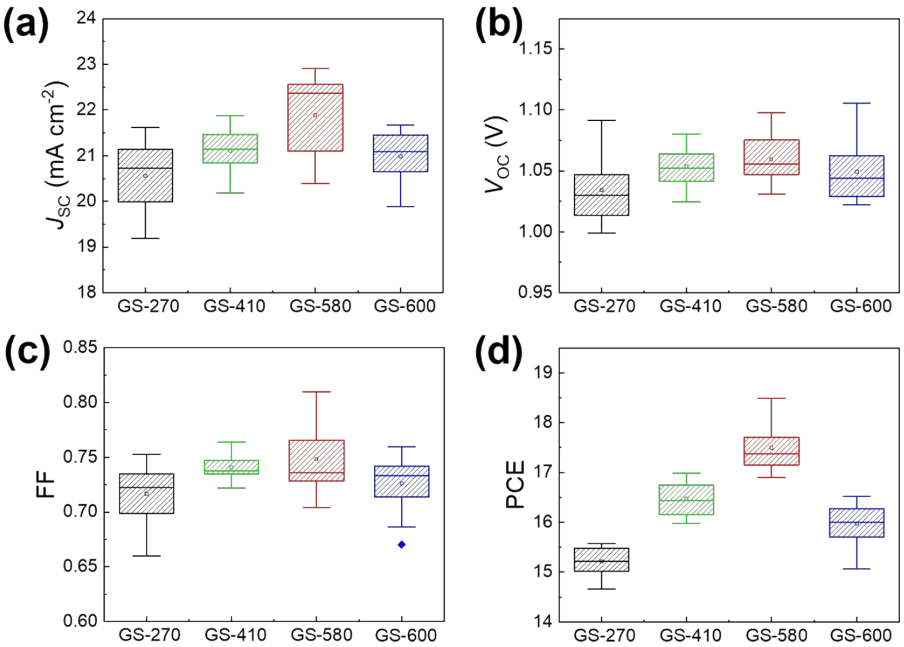

Fig. S8. Statistical parameters of (a) J_{SC}, (b) V_{OC}, (c) FF and (d) PCE for the PSCs based on perovskite films with different grain size. The data collected from 80 cells (20 cells for each type).

Table S4. Photovoltaic parameters of PSCs based on the perovskite films with different grain size.

Sample		V_{OC} (V)	J_{SC} (mA cm^{-2})	FF	PCE (%)
GS-270	best	1.04	19.99	0.73	15.57
	average	1.03 ± 0.07	20.56 ± 1.05	0.72 ± 0.03	15.22 ± 0.35
GS-410	best	1.05	21.87	0.74	16.99
	average	1.05 ± 0.03	21.11 ± 0.76	0.74 ± 0.01	16.50 ± 0.49
GS-480	best	1.07	22.15	0.78	18.49
	average	1.06 ± 0.05	22.23 ± 1.23	0.75 ± 0.06	17.50 ± 0.99

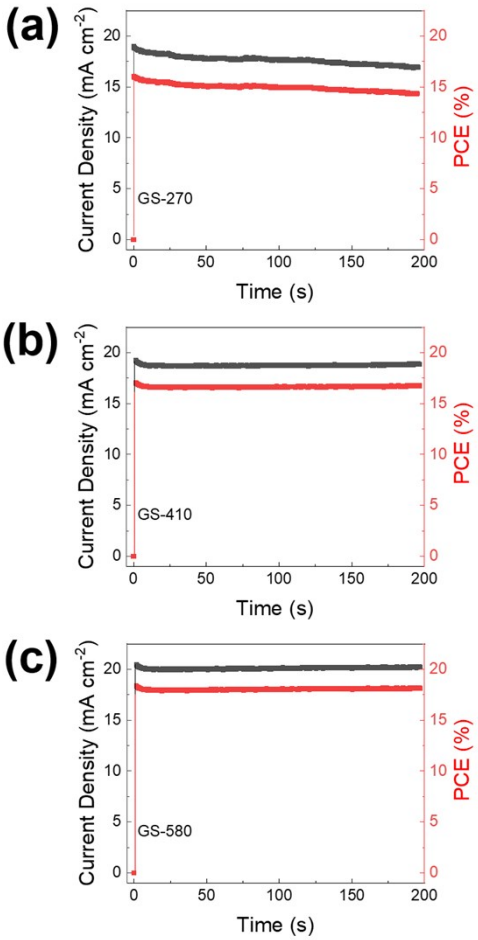

Fig. S9. Steady-state efficiency and photocurrent density output of (a) GS-270, (b) GS-410 and (c) GS-580 PSCs.

Table S5. The fitted parameters from EIS measurements.

Sample	R_s (Ω cm^{-2})	R_{rec} (kΩ cm^{-2})
GS-270 PSCs	226	108
GS-410 PSCs	203	413
GS-580 PSCs	167	695

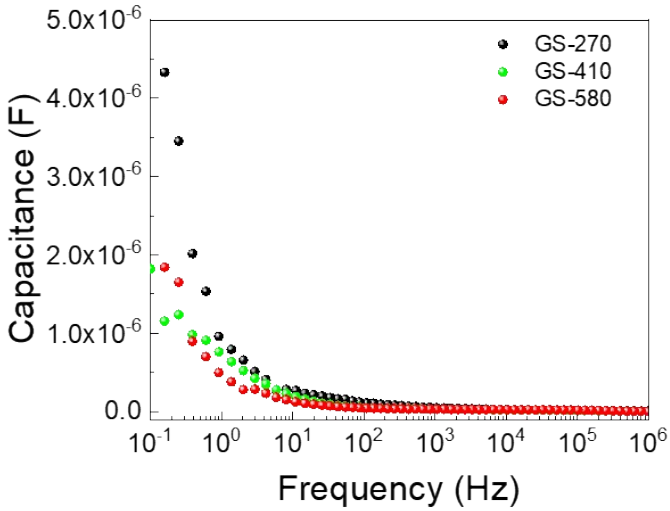

Fig. S10. Capacitance−frequency curves of PSCs based on perovskite films with different grain size.

The trap density of states (tDOS) can be derived from the equation:[13]

$$N_T(E_\omega) = -\frac{V_{bi}\, dC\ \ \omega}{qWd\omega k_B T} \qquad \text{S4}$$

where V_{bi} and W is the built-in potential and depletion width, respectively, and the V_{bi} and W reported in the literature are generally 1 V and 500 nm respectively.[14,15] q is the elementary charge, C is the capacitance, and ω is the applied angular frequency of perturbation, which defines an energetic demarcation expressed as equation,

$$E_\omega = k_B T \ln\left(\frac{v_0}{\omega}\right) \qquad \text{S5}$$

where the attempt-to-escape frequency v_0 is usually $2\times10^{11}s^{-1}$.[15]

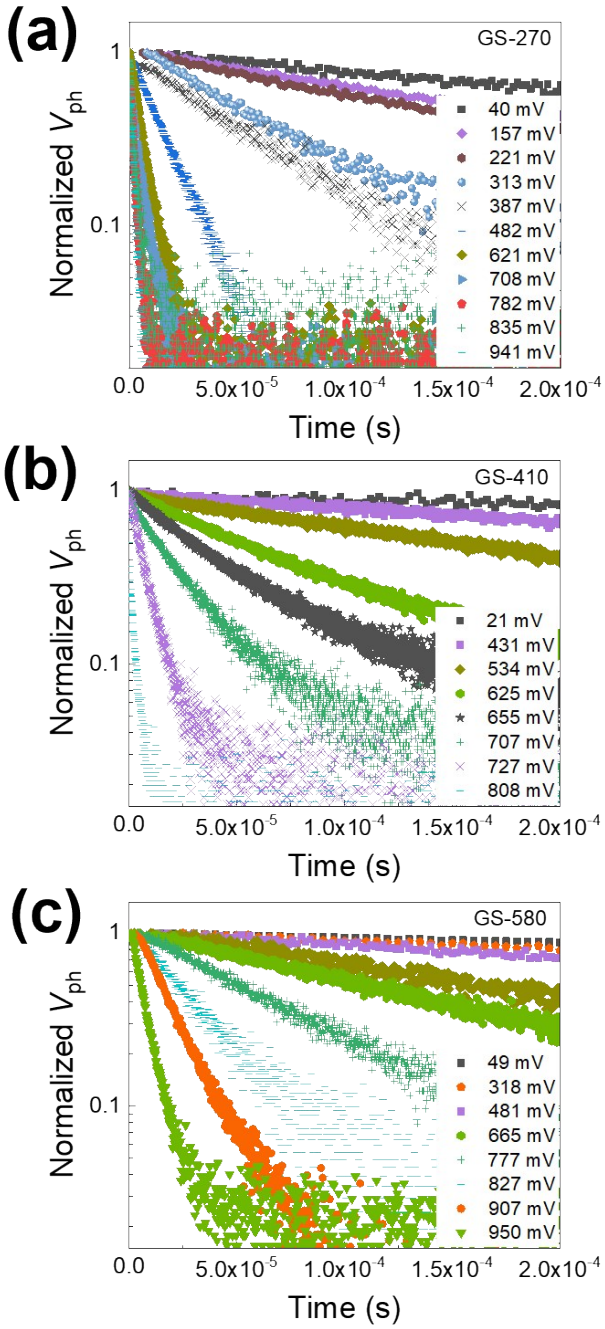

Fig. S11. The normalized TPV decay traces of diverse steady-state photovoltages of (a) GS-270, (b) GS-410 and (c) GS-540 PSCs.

The raw TPV data were fitted with bi-exponential decay equation,

$$V_{ph} = A_1 exp\left(-\frac{t}{\tau_1}\right) + A_2 exp(-\frac{t}{\tau_2}) \qquad \text{S6}$$

where A_1 and A_2 are pre-exponential factors, and τ_1 and τ_2 are time constants. The average charge recombination time constants (τ_r) are calculated as shown below,

$$\tau_r = \frac{A_1\tau_1 + A_2\tau_2}{A_1 + A_2} \qquad \text{S7}$$

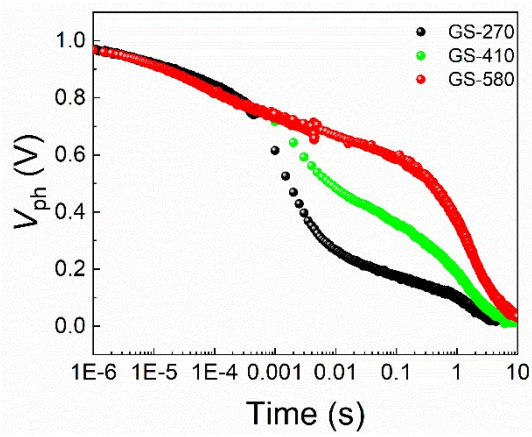

Fig. S12. OCVD curves of PSCs based on perovskite films with different grain size.

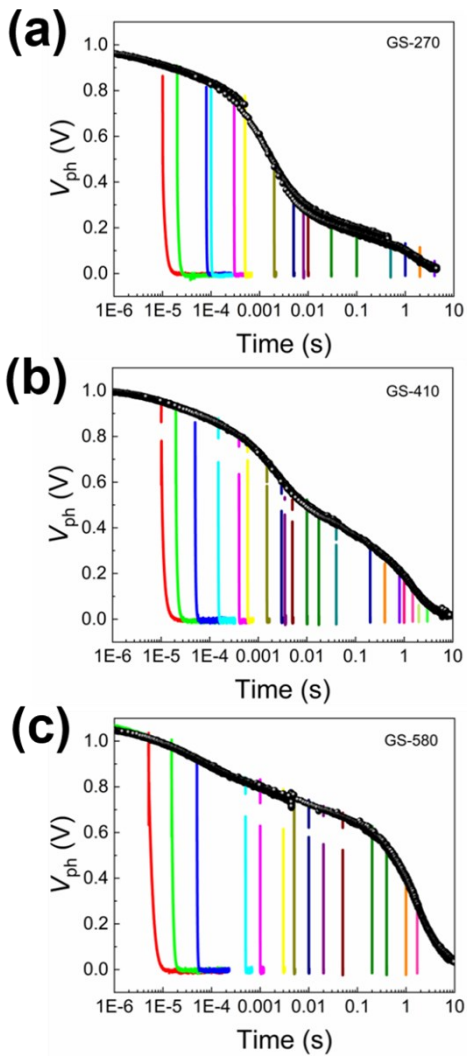

Fig. S13. Representative kinetics trace of the overall photovoltage (V_{ph}) for an open-circuit PSCs

device (black solid sphere), and the charge extraction kinetics at indicated timing (color lines) recorded by fast switching of the PSCs into short circuit.

References

1. D. Y. Son, S. G. Kim, J. Y. Seo, S. H. Lee, H. Shin, D. Lee and N. G. Park, Universal Approach toward Hysteresis-Free Perovskite Solar Cell via Defect Engineering, *J. Am. Chem. Soc.*, 2018, **140**, 1358-1364.
2. L. Xie, J. Chen, P. Vashishtha, X. Zhao, G. S. Shin, S. G. Mhaisalkar and N.-G. Park, Importance of Functional Groups in Cross-Linking Methoxysilane Additives for High-Efficiency and Stable Perovskite Solar Cells, *ACS Energy Lett.*, 2019, **4**, 2192-2200.
3. X. Huang, R. Chen, G. Deng, F. Han, P. Ruan, F. Cheng, J. Yin, B. Wu and N. Zheng, Methylamine-Dimer-Induced Phase Transition toward $MAPbI_3$ Films and High-Efficiency Perovskite Solar Modules, *J. Am. Chem. Soc.*, 2020, **142**, 6149-6157.
4. C. Fei, L. Guo, B. Li, R. Zhang, H. Fu, J. Tian and G. Cao, Controlled Growth of Textured Perovskite Films towards High Performance Solar Cells, *Nano Energy*, 2016, **27**, 17-26.
5. F. Ye, J. Ma, C. Chen, H. Wang, Y. Xu, S. Zhang, T. Wang, C. Tao and G. Fang, Roles of MACl in Sequentially Deposited Bromine-Free Perovskite Absorbers for Efficient Solar Cells, *Adv. Mater.*, 2020, **32**, 2007126.
6. D. H. Cao, C. C. Stoumpos, C. D. Malliakas, M. J. Katz, O. K. Farha, J. T. Hupp and M. G. Kanatzidis, Remnant PbI_2, an Unforeseen Necessity in High-Efficiency Hybrid Perovskite-Based Solar Cells, *APL Mater.*, 2014, **2**, 091101.
7. Y. Sun, Z. Zhou, Z. Huang, J. Wu, L. Zhou, Y. Cheng, J. Liu, C. Zhu, M. Yu, P. Yu, W. Zhu, Y. Liu, J. Zhou, B. Liu, H. Xie, Y. Cao, H. Li, X. Wang, K. Liu, X. Wang, J. Wang, L. Wang and W. Huang, Band Structure Engineering of Interfacial Semiconductors Based on Atomically Thin Lead Iodide Crystals, *Adv. Mater.*, 2019, **31**, 1806562.
8. J. Dai, H. Zheng, C. Zhu, J. Lu and C. Xu, Comparative Investigation on Temperature-Dependent Photoluminescence of $CH_3NH_3PbBr_3$ and $CH(NH_2)_2PbBr_3$

Microstructures, *J. Mater. Chem. C*, 2016, **4**, 4408-4413.

9. K. Wu, A. Bera, C. Ma, Y. Du, Y. Yang, L. Li and T. Wu, Temperature-Dependent Excitonic Photoluminescence of Hybrid Organometal Halide Perovskite Films, *Phys. Chem. Chem. Phys.*, 2014, **16**, 22476-22481.
10. Y. Liu, H. Lu, J. Niu, H. Zhang, S. Lou, C. Gao, Y. Zhan, X. Zhang, Q. Jin and L. Zheng, Temperature-Dependent Photoluminescence Spectra and Decay Dynamics of $MAPbBr_3$ and $MAPbI_3$ Thin Films, *AIP Adv.*, 2018, **8**, 095108.
11. A. D. Wright, C. Verdi, R. L. Milot, G. E. Eperon, M. A. Perez-Osorio, H. J. Snaith, F. Giustino, M. B. Johnston and L. M. Herz, Electron-Phonon Coupling in Hybrid Lead Halide Perovskites, *Nat. Commun.*, 2016, **7**, 11755.
12. H.-Y. Wang, M. Y. Hao, J. Han, M. Yu, Y. Qin, P. Zhang, Z. X. Guo, X.-C. Ai and J.-P. Zhang, Adverse Effects of Excess Residual PbI_2 on Photovoltaic Performance, Charge Separation, and Trap-State Properties in Mesoporous Structured Perovskite Solar Cells, *Chem. Eur. J.*, 2017, **23**, 3986-3992.
13. Y. Shao, Z. Xiao, C. Bi, Y. Yuan and J. Huang, Origin and Elimination of Photocurrent Hysteresis by Fullerene Passivation in $CH_3NH_3PbI_3$ Planar Heterojunction Solar Cells, *Nat. Commun.*, 2014, **5**, 5784.
14. Q. Dong, C. H. Y. Ho, H. Yu, A. Salehi and F. So, Defect Passivation by Fullerene Derivative in Perovskite Solar Cells with Aluminum-Doped Zinc Oxide as Electron Transporting Layer, *Chem. Mater.*, 2019, **31**, 6833-6840.
15. M. Samiee, S. Konduri, B. Ganapathy, R. Kottokkaran, H. A. Abbas, A. Kitahara, P. Joshi, L. Zhang, M. Noack and V. Dalal, Defect Density and Dielectric Constant in Perovskite Solar Cells, *Appl. Phys. Lett.*, 2014, **105**, 153502.